Spin cycloid quenching in Nd^{3+}-substituted BiFeO_{3}

P. Chen, Ö. Günaydın-Şen, W. J. Ren, Z. Qin, T. V. Brinzari, S. McGill, S.-W. Cheong, and J. L. Musfeldt

Phys. Rev. B **86**, 014407 — Published 10 July 2012

DOI: 10.1103/PhysRevB.86.014407

Spin cycloid quenching in Nd^{3+}-substituted $BiFeO_3$

P. Chen,[1] Ö. Günaydın-Şen,[1] W. J. Ren,[2,3] Z. Qin,[2,4] T. V. Brinzari,[1] S. McGill,[5] S. -W. Cheong,[2] and J. L. Musfeldt[1]

[1]*Department of Chemistry, University of Tennessee, Knoxville, TN 37996, USA*
[2]*Department of Physics, Rutgers University, Piscataway, NJ 08854, USA*
[3]*Shenyang National Laboratory for Materials Science, Institute of Metal Research, Chinese Academy of Sciences, Shenyang 110016, PRC*
[4]*New Jersey Institute of Technology, Newark, NJ 07102, USA*
[5]*National High Magnetic Field Laboratory, Tallahassee, FL 32310, USA*

(Dated: June 6, 2012)

Chemical substitution is an effective method for tailoring the electronic and magnetic properties of functional materials. In this work, we employ magneto-optical spectroscopy to investigate the behavior of the cycloid → homogenous (canted antiferromagnet) ordering transition in $Bi_{1-x}Nd_xFeO_3$. From the magneto-optical response, we construct a B–T–x phase diagram that shows how the critical field decreases with Nd^{3+} substitution, an effect that we model with Ginzburg-Landau free energy and harmonic cycloid approximations. Compared with non-magnetic impurities like La^{3+}, Nd^{3+} is a stronger quencher and yields non-linear B_C–x behavior. Spiral magnetic order is quenched when x∼0.2. With increasing temperature (T<90 K), the critical field rises gently, a consequence of magnetic anisotropy changes with temperature. These findings extend our understanding of charge-spin coupling and advance the development of magnetic ferroelectrics.

PACS numbers: 75.30.Kz, 75.50.Ee, 78.20.Bh, 78.20.Ls

Single phase materials that simultaneously expose both ferroelectricity and ferromagnetism have been challenging to realize. This is because of the mutually exclusive mechanisms for these two properties: standard ferroelectricity in cubic perovskites requires empty d orbitals whereas ferromagnetism derives from partially filled d orbitals[1,2]. One way forward is to select a parent compound with several desirable characteristics and to employ chemical or physical tuning to bring in the missing features. Chemical substitution is a well-known strategy for tuning the physical properties of a material[3–8] and is a promising route for achieving the desired multifunctionality[9,10]. This strategy is backed by the recent prediction that a magnetic ion placed on the perovskite "A site" may activate ferroelectrically-induced ferromagnetism due to coupling between the Jahn-Teller distortion and weak canting[11,12].

In this work, we focus on the rhombohedrally distorted perovskite $BiFeO_3$. This system is different than traditional cubic perovskites. Ferroelectricity below 1100 K derives from the Bi^{3+} 6s lone pairs[13,14], and G-type antiferromagnetism below 640 K is due to the non-collinear arrangement of Fe^{3+} spins[15,16]. $BiFeO_3$ displays an $R3c$ lattice[17] that is very amenable to chemical substitution[18]. Among the many types of substitution under investigation[4,5,7,18,19], those that yield both ferroelectricity and ferromagnetism are especially attractive due to possible magnetoelectric device applications[20]. $Bi_{1-x}Nd_xFeO_3$ in the range of $0.15 \leq x \leq 0.175$ is a physical realization of this important case[18]. In this system, the remnant polarization decreases from ∼9 $\mu C/cm^2$ in $BiFeO_3$ to 0 at x=0.20 due to reduced Bi^{3+} lone pair activity[18]. At the same time, the remnant magnetization increases to 0.227 emu/g at x=0.20. At low temperature, magnetic order in $BiFeO_3$ is modulated by a cycloidal spiral propagating along $[110]_{hex}$ with a period of ∼620 Å[21]. This spiral order can be suppressed by magnetic field (B_C∼20 T)[22,23] resulting in a canted antiferomagnetic structure[24], and the domain structure can be modified with uniaxial strain[25]. Field induced polarization work indicates a 10 T critical field with 10% Nd^{3+} replacement[26], demonstrating that chemical substitution impacts spin spiral order as well. Naturally, many oxide multiferroics have been investigated by spectroscopic techniques. In $BiFeO_3$, certain features are very sensitive to variations in magnetic order and can be used to reveal the fundamental charge-spin coupling mechanism.[23,27]

In this report, we combine magneto-optical spectroscopy with a suite of $Bi_{1-x}Nd_xFeO_3$ materials to more deeply explore the physics of spin spiral quenching. With magnetic field-induced changes in the underlying magnon sideband as our probe of spin spiral behavior, we find that the critical field decreases with Nd^{3+} substitution, an effect that can be understood in terms of a larger anisotropy constant, longer spiral wavelength, and increased magnetic susceptibility. On the contrary, temperature (T<90 K) stabilizes the spin spiral phase, a consequence of magnetic anisotropy changes with temperature. We bring these results together to create a comprehensive B-T-x phase diagram and discuss the combined effect of magnetic field and chemical substitution. The superposition creates a broad tranche of phase space where polarization survives and the spin spiral is either eliminated or can be suppressed with modest fields. This work advances the fundamental understanding of charge-spin coupling and the development of multiferroic materials with coexisting ferroelectricity and ferromagnetism.

A series of polycrystalline $Bi_{1-x}Nd_xFeO_3$ ceramics with x = 0, 0.03, 0.07, 0.09, 0.10, 0.15, and 0.20 was prepared by the solid-state sintering route from Fe_2O_3,

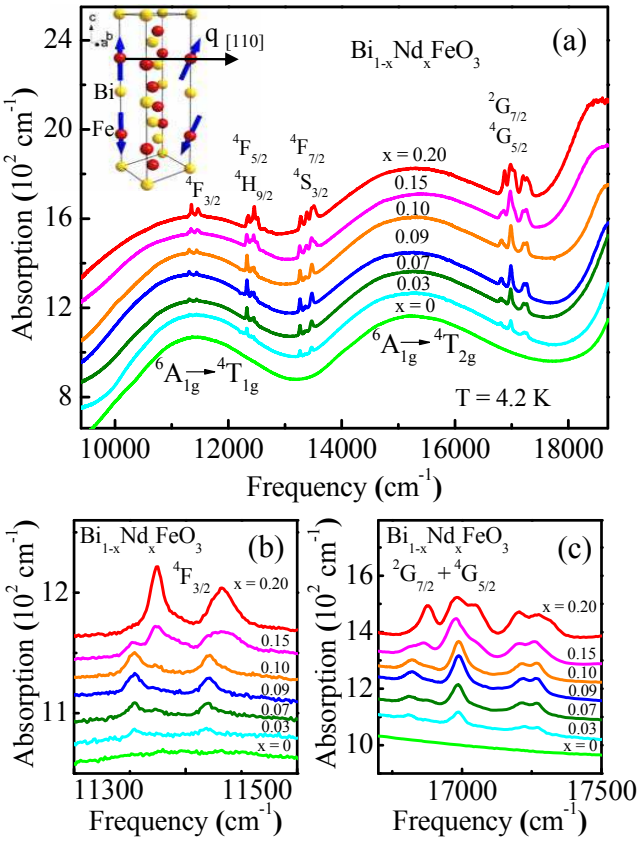

FIG. 1: (Color online) (a) Absorption coefficient of $Bi_{1-x}Nd_xFeO_3$ ($0 \leq x \leq 0.20$) in the range of the on-site Fe^{3+} d-d excitations at 4.2 K. The spectra of the substituted compounds are offset along the y-axis for clarity. The sharp structures riding on top of the color band excitations are the well-known Nd^{3+} $4f$ excitations from the $^4I_{9/2}$ ground state to various excited states. They are labeled according to Refs.[23,28]. Inset: structure of $BiFeO_3$ hexagonal unit cell. Only the Bi and Fe atoms are displayed for clarity. Spin spiral propagation (q) is along the $[110]_{hex}$ direction. (b, c) Close-up view of these excitations at different Nd^{3+} concentrations. Panel (b) shows the $^4I_{9/2} \rightarrow {}^4F_{3/2}$ features whereas panel (c) displays the $^4I_{9/2} \rightarrow {}^2G_{7/2}+{}^4G_{5/2}$ excitations.

Bi_2O_3, and Nd_2O_3. Spectra were collected using a Bruker Equinox 55 Fourier transform infrared spectrometer equipped with a microscope attachment (600–17000 cm^{-1}; 1 cm^{-1} resolution). The absorption coefficient was calculated as $\alpha(\omega) = -\frac{1}{d} lnT(\omega)$, where d is the thickness, and $T(\omega)$ is the measured transmittance. Temperature control was achieved with an open-flow cryostat. Magneto-optical measurements were carried out with McPherson 2061A monochromator at the NHMFL using a resistive magnet (0-35 T; 4.2-90 K; 7000-40000 cm^{-1}). We focus on the 9500-11000 cm^{-1} range, a choice driven by the physics of $BiFeO_3$ as discussed below. Absorption difference spectra were calculated as $\triangle\alpha = [\alpha(B) - \alpha(B = 0\ T)]$. We identified the magnetic phase boundaries using slope discontinuities in the oscillator strength trends of the absorption difference spectra. These optical results allow us to construct a B–T–x phase diagram. Traditional peak fitting methods were employed as appropriate.

Figure 1(a) displays the 4.2 K absorption spectra of $Bi_{1-x}Nd_xFeO_3$ ($0 \leq x \leq 0.20$). We assign the two strong bands centered at ~11200 and 15250 cm^{-1} in the end member as $^6A_{1g} \rightarrow {}^4T_{1g}$ and $^6A_{1g} \rightarrow {}^4T_{2g}$ on-site excitations of Fe^{3+}[23,29]. These d–d excitations are formally spin and parity forbidden. They are activated in $BiFeO_3$ and other transition metal oxides by spin-orbit coupling, exchange interaction, and odd parity phonons that hybridize states and break inversion symmetry[30]. The sharp structures superimposed on the d-d bands provide evidence of Nd^{3+} incorporation. The intensity increases with chemical substitution, and the line pattern depends upon the crystal field around the rare earth center. We assign these features as $4f$ excitations from the $^4I_{9/2}$ ground state to various excited states as indicated in Fig. 1(a)[28]. Naturally, the rare earth excitations in $Bi_{1-x}Nd_xFeO_3$ are very sensitive to the local structure[31]. Figures 1(b) and (c) display close-up views of the well-known $^4I_{9/2} \rightarrow$ metastable $^4F_{3/2}$ and $^4I_{9/2} \rightarrow {}^2G_{7/2}+{}^4G_{5/2}$ exitations[28]. Compared with the features in the $x \leq 0.10$ sample, the two peaks assigned as $^4I_{9/2}(0) \rightarrow {}^4F_{3/2}(0)$ and $^4I_{9/2}(0) \rightarrow {}^4F_{3/2}(1)$ [Fig. 1(b)][34] start to disappear at x=0.15 and two new features with higher energy emerge at x=0.20; the separation also decreases by ~14 cm^{-1}. Moreover, the peaks centered at 16,988 and 17,270 cm^{-1} split into doublets at x=0.20 [Fig. 1(c)]. These effects are due to distortion of the Nd^{3+} crystal field, a consequence of the structural change from rhombohedral in pristine $BiFeO_3$ → rhombohedral with slight triclinic distortion ($0.05 \leq x \leq 0.10$) → pseudo-tetragonal ($x \geq 0.20$)[18].

Antiferromagnets have traditionally offered foundational opportunities to investigate the collective excitations that arise from charge-spin coupling[35]. The magnon sideband is one of these well-known excitations. It arises from the combination of an exciton and a magnon and is commonly observed on the leading edge of the first d–d band in antiferromagnets like MnF_2 and α-Fe_2O_3[29,36]. Interestingly, the magnon sideband is not clearly evident in the linear absorption spectrum of single crystalline $BiFeO_3$[23,37]. This is because the center of symmetry between Fe^{3+} centers suppresses the transition of exchange coupled pairs[39]. Similarly, the magnon sideband is not directly observed in polycrystalline $Bi_{1-x}Nd_xFeO_3$ [Fig. 1(a)], though it is likewise expected. Our previous magneto-optical work on single crystalline $BiFeO_3$ finessed this situation, revealing underlying magnon sideband features in the magneto-optical response[23]. It is clearly very attractive to extend this technique to systems like $Bi_{1-x}Nd_xFeO_3$ where chemical substitution stabilizes weak ferromagnetism at the expense of the antiferromagnetic (spin spiral) phase. But here, the magnon sideband is both hidden and potentially contaminated with Nd^{3+} excitations[40]. Based

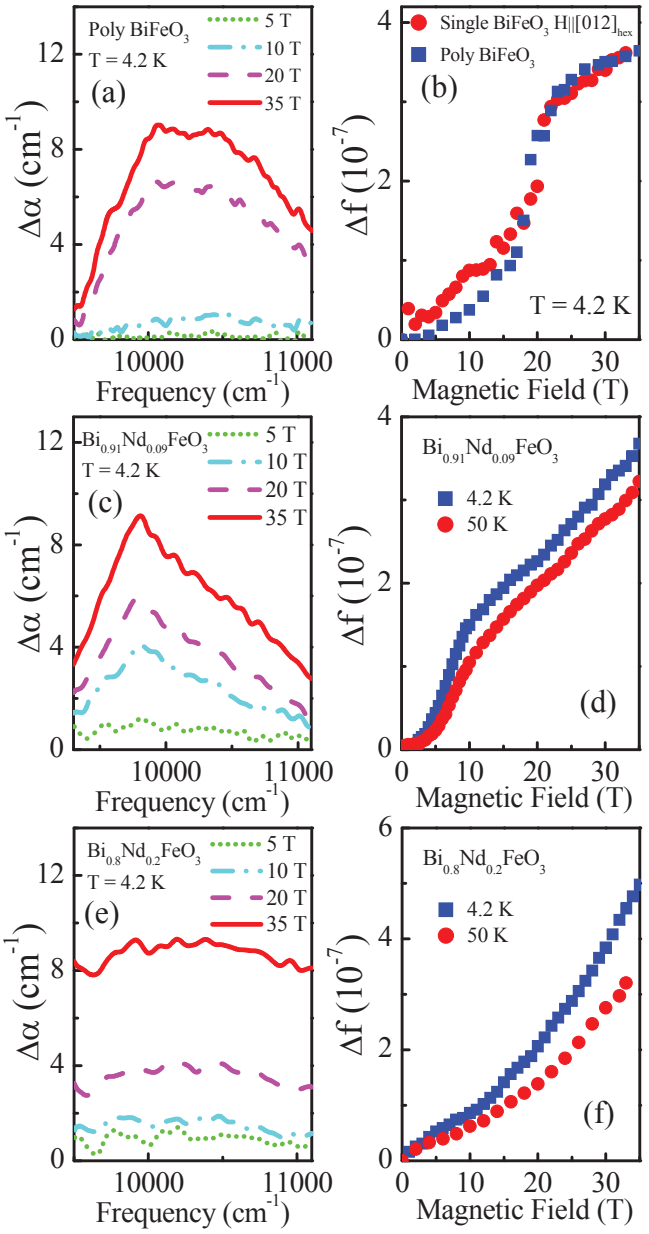

FIG. 2: (Color online) Absorption difference spectra $\triangle\alpha$=[$\alpha(B) - \alpha(B = 0$ T)] of $Bi_{1-x}Nd_xFeO_3$ at 4.2 K for selected Nd^{3+} concentrations: (a) x=0, (c) x=0.09, and (e) x=0.20. (b) Comparison of oscillator strength change ($\triangle f$) in polycrystalline and single crystalline $BiFeO_3$[23] in the magnon sideband range as a function of applied magnetic field. (d, f) Comparison of oscillator strength change ($\triangle f$) at selected temperatures (4.2 and 50 K) for (d) x=0.09 and (f) x=0.20.

on our previous work with pristine $BiFeO_3$[23], a portion of the field-induced magnon sideband-related changes appear between 9500 and 11000 cm^{-1}, a regime where Nd^{3+} excitations are absent. Magnetochromism in this range therefore provides an an excellent opportunity to investigate how local magnetism (introduced by rare earth substitution) impacts the antiferromagnetic spin spiral state.

Figure 2 summarizes the magneto-optical response of $Bi_{1-x}Nd_xFeO_3$. Panels (a), (c), and (e) display the field-induced absorption difference spectra for x=0.0, 0.09 and 0.20, substitutions that correspond to rhombohedral, triclinic, and pseudo-tetragonal crystal structures, respectively. Different magneto-optical contrast is observed depending on the Nd^{3+} concentration, an indication of magnon sideband sensitivity to competing local and long-range magnetic interactions[41]. The magnon sideband intensity also increases with magnetic field. We quantified these effects with the oscillator strength sum rule[42]: $\Delta f \equiv \frac{2c}{N_e \pi \omega_p^2} \int_{\omega_1}^{\omega_2} n\Delta\alpha(\omega, B)\, d\omega$. Here, f is the oscillator strength, N_e=5 is the number of electrons per Fe^{3+} site, $n \simeq 2.7$ is the refractive index[43], ω_p is the plasma frequency$\equiv\sqrt{\frac{e^2\rho}{m\epsilon_0}}$, e and m are the charge and mass of an electron, ϵ_0 is the vacuum dielectric constant, ρ is the density of Fe sites[18], c is the speed of light, and ω_1=9500 cm^{-1} and ω_2=11000 cm^{-1} are the frequency limits of integration. Δf of polycrystalline $BiFeO_3$ displays a broad increase in the 17-26 T range [Fig. 2(b)], different from the sharp jump at 20 T[22,23] in $(012)_{hex}$ face single crystals. The latter can be unambiguously assigned as the field-induced spin spiral quenching transition that drives toward a homogeneous canted antiferromagnetic state above the critical field (B_C)[22]. Orientational averaging of the easy and hard magnetization axes accounts for the broad transition region in polycrystalline $BiFeO_3$[22,44,45]. As shown in Figs. 2(d) and 2(f), increasing temperature also reduces Δf, a trend that is probably related to the approach of the 140 K spin-reorientation transition[46,47]. The temperature-induced reduction of Δf is larger at higher rare earth substitution levels, a result that we attribute to Nd^{3+}-Fe^{3+} interactions. In principle, f follows phonon assisted trends[23], so Δf is expected to increase at high temperature (T>250 K). At x=0.20, we find only a smooth increase in Δf with no optical signature of the field-induced transition. This indicates that spiral order is suppressed in $Bi_{0.80}Nd_{0.20}FeO_3$. Antiferromagnetic sublattice canting[48,49] instead results in weak ferromagnetism[18].

We combined these magneto-optical results to generate the B–T–x diagram of $Bi_{1-x}Nd_xFeO_3$ [Fig. 3(a)]. At low magnetic fields and modest Nd^{3+} incorporation levels, $BiFeO_3$ and the chemically-substituted analogs possess spiral magnetic order as indicated by the blue shading. At the other extreme, high magnetic field[23,26] and additional rare earth substitution quench the spin spiral and strongly stabilize the homogeneous magnetic state. The latter is indicated in red. The transition region (shown in yellow) is broadened due to orientational averaging effects. As discussed below, two-dimensional cross sections of this B–T–x diagram (at fixed temperature and composition) reveal the important trends more clearly.

Figure 3(b) summarizes the B–x behavior of $Bi_{1-x}Nd_xFeO_3$ at 4.2 K. With substitution, the critical field demarcated by the yellow transition region decreases systematically. The Ginzburg-Landau free en-

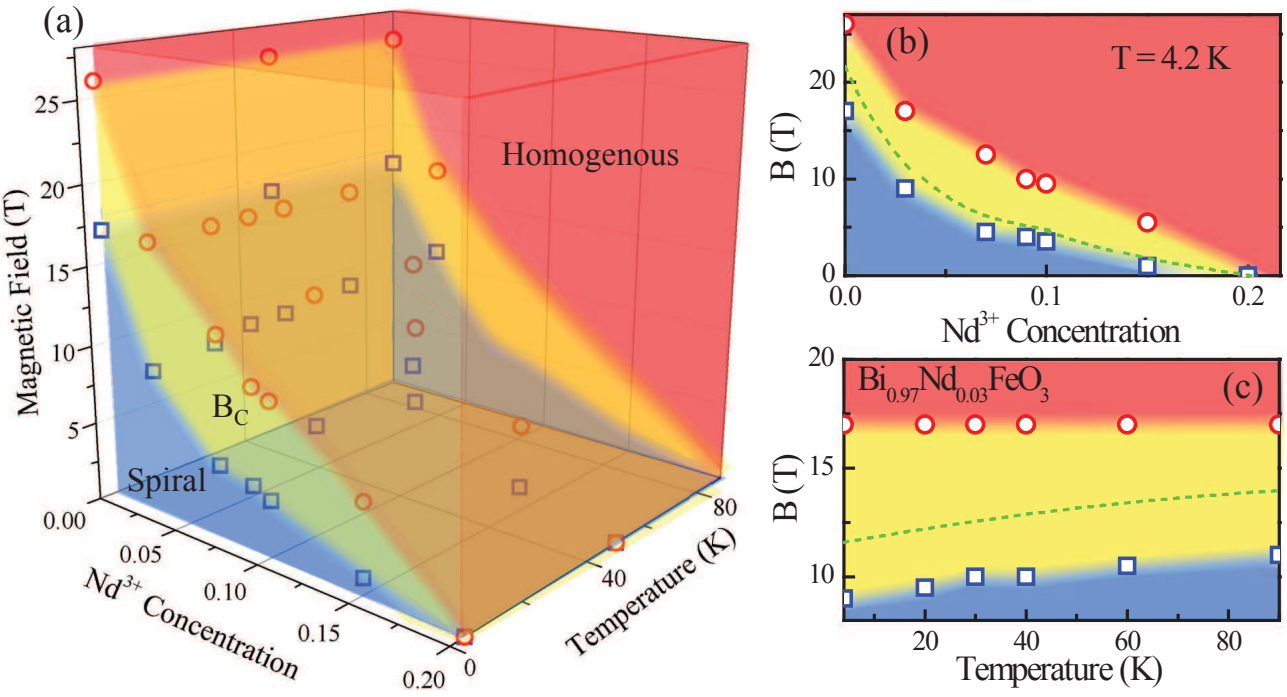

FIG. 3: (Color online) (a) B–T–x phase diagram of $Bi_{1-x}Nd_xFeO_3$ constructed using change in oscillator strength ($\triangle f$) data in the range of the magnon sideband. Panels (b) and (c) show Nd^{3+} concentration and temperature slices taken from this three-dimensional plot. The B–x diagram is at 4.2 K, and the B–T plot is for x=0.03. The blue squares indicate the phase boundary between spiral magnetic ordering and transition region, the red circles represent the phase boundary between transition region and homogeneous magnetic ordering. Error bars of these boundaries are smaller than the symbol size and not shown. The mean value of the transition region is indicated by the green dashed lines.

ergy and harmonic cycloid approximation[8,22,50] provide a framework within which we can understand this trend. For a randomly oriented material, an applied field with arbitrary orientation results in a broad critical field region. We set $[001]_{hex}$ as the z axis, and the spin spiral propagation direction $[110]_{hex}$ as the y axis. Our calculation follows the work of Le Bras *et al.*[8]. When the magneto-electric induced effective field ($B_{ME}=m_s/\chi_\perp$) is small compared with the critical field along the z axis ($B_{C,z}=\sqrt{\frac{4(Aq^2-\frac{|K|}{2})}{\chi_\perp}}$), a minimum critical field can be obtained when field is along the y axis:

$$B_{C,min}=\frac{2m_s}{\chi_\perp}(-1+\sqrt{\frac{3}{4}+\frac{\chi_\perp(Aq^2-\frac{|K|}{2})}{m_s^2}}). \quad (1)$$

Here, A is the exchange stiffness constant, K is the uniaxial anisotropy constant in zero field, m_s is the magneto-electric induced magnetization, $\chi_\perp$ is the magnetic susceptibility in the direction perpendicular to the antiferromagnetic vector, and q is the wave vector. When field is along the x axis, B_C reaches a maximum:

$$B_{C,max}=\frac{Aq^2-\frac{|K|}{2}}{m_s}-\frac{m_s}{4\chi_\perp}. \quad (2)$$

$B_{C,min}$ and $B_{C,max}$ correspond to the lowest and highest boundaries of the yellow transition region in Fig. 3(b), respectively. In $BiFeO_3$, $K \ll Aq^2$[22] and can be neglected. Using the reported values of $\chi_\perp=4.7\times10^{-5}$[22,50], $q=\frac{2\pi}{\lambda}$(λ=620 Å)[44], m_s = 2.56 emu/cm^3[22] and A=8.0 $\times10^{-7}$ erg/cm[50], we find $B_{C,min}$=17 T and $B_{C,max}$=30 T for pristine $BiFeO_3$. These predicted values are in excellent agreement with our magneto-optical results. Chemical substitution has important effect on the anisotropy constant. Experimentally, we find that $B_{C,min}$=3.5 T and $B_{C,max}$=9.5 T for $Bi_{0.90}Nd_{0.10}FeO_3$. Using $\chi_\perp=7.2\times10^{-5}$[18] and λ=680 Å (under the assumption that spiral wavelength typically increases by ~10% with low levels of substitution[6]), we estimate that m_s is ~0.5 emu/cm^3. Assuming exchange stiffness remains the same, we find $|K| = 1.3\times10^6$ erg/cm^3. These results agree reasonably with the estimates from electron spin resonance and magnetization[8,50]. The value of K is comparable to Aq^2, therefore, we conclude that anisotropy constant increases with Nd^{3+} ions substitution. As a further self-consistency check, we calculated B_{ME} and $B_{C,z}$ for $x \leq 0.10$ using Eqns. 1, 2 and found B_{ME} is less than 4% of $B_{C,z}$, confirming the validity of our approach. Moreover, we can obtain the mean value of critical field by using our estimated m_s and K and averaging over all applied field orientations. This quantity is plotted as a function of x and T as a green dashed line in Figs. 3(b) and (c). These curves fall well within the transition region mapped out by our spectroscopic work,

demonstrating the effectiveness of these expressions in explaining critical field phase boundary behavior[51]. Finally, we point out that the exponential decay of $B_{C,ave}$ is much faster than the linear decay revealed by La^{3+} substitution[8], an effect that emanates from magnetic interactions between between Fe^{3+} and Nd^{3+} centers.

Figure 3(c) displays the B–T behavior of $Bi_{0.97}Nd_{0.03}FeO_3$. This fixed composition slice of the three-dimensional phase diagram at $x = 0.03$ is useful for understanding how temperature impacts magnetic anisotropy and the critical field. With increasing temperature, the spiral $\rightarrow$ crossover regime boundary increases whereas that between the crossover regime and homogeneous magnetic phase is relatively constant. These trends combine to stabilize the spin spiral phase at the expense of the crossover regime, in excellent agreement with the field induced polarization result[26]. Reduced magnetic susceptibility over this temperature range along with an increasingly important $\chi_{\parallel}$ (typical of antiferromagnets) is probably behind this progression[52,53]. At much higher temperatures (but still below T_N), the increased susceptibility will lead to a lower critical field[52]. Moreover, $\chi_{\parallel}$ will approach $\chi_{\perp}$, which drives $B_{C,min}$ towards $B_{C,max}$. Temperature is thus expected to reduce the width of the transition regime, ultimately condensing it to a slice.

In summary, we employed magneto-optical spectroscopy to investigate the spiral order $\rightarrow$ homogeneous state transition in chemically-substituted $BiFeO_3$. The B–T–x diagram reveals precisely how the critical field decreases with rare earth substitution, a trend that destabilizes the antiferromagnetic spiral phase. The magneto-optical contrast degrades with increasing Nd^{3+} substitution, and in $Bi_{0.80}Nd_{0.20}FeO_3$, no field-induced optical signature, indicative of magnon sideband changes, is observed. This demonstrates that spiral magnetic order is quenched when $x{\sim}0.20$. The Ginzburg-Landau free energy allows us to understand this trend as the combined effect of larger anisotropy constant, longer spiral wavelength, and increased susceptibility. Nd^{3+} is shown to be more effective in quenching the spin spiral compared with La^{3+}. In contrast, temperature stabilizes the spin spiral phase, at least in the region of our investigation ($T{\leq}90$ K). These findings demonstrate that chemical substitution can help control field-induced magnetic ordering transitions, opening up a variety of possibilities for novel spintronic and magneto-optical device components.

This work was supported by the Materials Science Division, Basic Energy Sciences, U. S. Department of Energy (Contract Nos. DE-FG02-01ER45885 at the University of Tennessee (JLM) and DE-FG02-07ER46382 at Rutgers University (SWC)) and the National Science Foundation (DMR-0654118 at the National High Magnetic Field Laboratory (SMG)). We thank G. Le Bras for useful discussions.

[1] N. A. Hill, J. Phys. Chem. B **104**, 6694 (2000).
[2] S. W. Cheong and M. Mostovoy, Nat. Mater. **6**, 13 (2007).
[3] C. -H. Yang, J. Seidel, S. Y. Kim, P. B. Rossen, P. Yu, M. Gajek, Y. H. Chu, W. Martin, M. B. Holcomb, Q. He, P. Maksymovych, N. Balke, S. V. Kalinin, A. P. Baddorf, S. R. Basu, M. L. Scullin, and R. Ramesh, Nature Mater. **8**, 485 (2009).
[4] C. J. Cheng, D. Kan, S. H. Lim, W. R. McKenzie, P. R. Munroe, L. G. Salamanca-Riba, R. L. Withers, I. Takeuchi, and V. Nagarajan, Phys. Rev. B **80**, 014109 (2009).
[5] C. J. C. Bennett, H. S. Kim, M. Varela, M. D. Biegalski, D. H. Kim, D. P. Norton, H. M. Meyer, and H. M. Christen, J. Mater. Res. **26**, 132 (2011).
[6] I. Sosnowska, W. Schäfer, W. Kockelmann, K. H. Andersen, and I. O. Troyanchuk, Appl. Phys. A: Mater. Sci. Process. **74**, s1040 (2002).
[7] X. S. Xu, J. F. Ihlefeld, J. H. Lee, O. K. Ezekoye, E. Vlahos, R. Ramesh, V. Gopalan, X. Q. Pan, D. G. Schlom, and J. L. Musfeldt, Appl. Phys. Lett. **96**, 192901 (2010)
[8] G. Le Bras, D. Colson, A. Forget, N. Genand-Riondet, R. Tourbot, and P. Bonville, Phys. Rev. B **80**, 134417 (2009).
[9] Y. Matsumoto, M. Murakami, T. Shono, T. Hasegawa, T. Fukumura, M. Kawasaki, P. Ahmet, T. Chikyow, S. Koshihara, and H. Koinuma, Science **291**, 854 (2001).
[10] H. Y. Hwang, S.-W. Cheong, P. G. Radaelli, M. Marezio, and B. Batlogg, Phys. Rev. Lett. **75**, 914 (1995).
[11] C. Ederer and C. J. Fennie, J. Phys.: Condens. Matter **20**, 434219 (2008).
[12] C. J. Fennie, Phys. Rev. Lett. **100**, 167203 (2008).
[13] R. Seshadri and N. A. Hill, Chem. Mater. **13**, 2892–2899 (2001).
[14] J. B. Neaton, C. Ederer, U. V. Waghmare, N. A. Spaldin, and K. M. Rabe, Phys. Rev. B. **71**, 014113 (2005).
[15] J. R. Teague, R. Gerson, and W. J. James, Solid State Commun. **8**, 1073 (1970).
[16] S. V. Kiselev, R. P. Ozerov, and G. S. Zhdanov, Sov. Phys. Dokl. **7**, 742 (1963).
[17] P. Fischer, M. Polomska, I. Sosnowska, and M. Szymanskig, J. Phys. C: Sol. Stat. Phys. **13**, 1931 (1980).
[18] G. L. Yuan, S. W. Or, J. M. Liu, and Z. G. Liu, Appl. Phys. Lett. **89**, 052905 (2006).
[19] H. M. Christen, J. H. Nam, H. S. Kim, A. J. Hatt, and N. A. Spaldin, Phys. Rev. B **83**, 144107 (2011).
[20] M. Fiebig, J. Phys. D **38**, R123 (2005).
[21] I. Sosnowska, T. Peterlin-Neumaier, and E. Steichele, J. Phys. C:Solid State Phys. **15**, 4835 (1982).
[22] A. M. Kadomtseva, A. K. Zvezdin, Y. F. Popov, A. P. Pyatakov, and G. P. Vorob'ev, Jetp Lett. **79**, 571 (2004).
[23] X. S. Xu, T. V. Brinzari, S. Lee, Y. H. Chu, L. W. Martin, A. Kumar, S. McGill, R. C. Rai, R. Ramesh, V. Gopalan, S. -W. Cheong, and J. L. Musfeldt, Phys. Rev. B. **79**, 134425 (2009).
[24] The homogeneous phase is a collinear phase, but spin is canted due to the Dzyaloshinski-Moriya effect, resulting in weak ferromagnetism.
[25] M. Ramazanoglu, W. Ratcliff, H. T. Yi, A. A. Sirenko, S. -W. Cheong, and V. Kiryukhin, Phys. Rev. Lett. **107**, 067203 (2011).
[26] A. Kadomtseva, Yu. Popov, G. Vorob'ev, and A. Zvezdin, Physica B **211**, 327 (1995).
[27] T. T. A. Lummen, P. Chen, M. O. Ramirez, E. A. Barnes, N. J. Podraza, J. L. Musfeldt, V. Gopalan,Optical probing of spin-charge-lattice coupling in multiferroics, in Multiferroics, L. W. Martin, R. Ramesh, eds., (Wiley, in press).
[28] R. Balda, M. Sanz, A. Mendioroz, J. Fernández, L. S. Griscom, and J.-L. Adam, Phys. Rev. B **64**, 144101 (2001).
[29] P. Chen, N. Lee, S. McGill, S. -W. Cheong, and J. L. Musfeldt, Phys. Rev. B **85**, 174413 (2012).
[30] L. L. Lohr, Coord. Chem. Rev. **8**, 241 (1972).
[31] Since Nd^{3+} replaces the Bi^{3+} centers in these solid solutions, the local structure for low levels of rare earth incorporation is octahedral[32]. At very high subsitutition levels, the local field is expected to approach the 8-fold square antiprismatic environment of the $NdFeO_3$ end member[33].
[32] L. W. Finger and R. M. Hazen, J. Appl. Phys. **51**, 5362 (1980).
[33] W. Sławiński, R. Przeniosło, I. Sosnowska, and E. Suard, J. Phys.: Condens. Matter **17**, 4605 (2005).
[34] X. S. Xu, T. V. Brinzari, S. McGill, H. D. Zhou, C. R. Wiebe, and J. L. Musfeldt, Phys. Rev. Lett. **103**, 267402 (2009).
[35] D. D. Sell, R. L. Greene, and R. M. White, Phys. Rev. **158**, 489 (1967).
[36] R. L. Greene, D. D. Sell, W. M. Yen, and A. L. Schawlow, Phys. Rev. Lett. **15**, 656 (1965).
[37] They do, however have a signature in second harmonic generation spectra[38]
[38] M.O. Ramirez, A. Kumar, S.A. Denev, N. J. Podroza, X.S. Xu, R.C. Rai, Y.H. Chu, J. Seidel, L. W. Martin, S.-Y. Yang, E. Saiz, J.F. Ihlefeld, S. Lee, J. Klug, S.-W. Cheong, M.J. Bedzyk, O. Auciello, D.G. Schlom, R. Ramesh, J. Orenstein, J.L. Musfeldt, and V. Gopalan, Phys. Rev. B. **79**, 224106 (2009).
[39] Y. Tanabe, T. Moriya, S. Sugano, Phys. Rev. Lett. **15**, 1023 (1965).
[40] This is a challenge for optical properties work as well as for bulk magnetization measurements, since rare earth excitations can interfere with the interpretation of the latter.[34]
[41] J. Bartolome, E. Palacios, M. D. Kuzmin, F.Bartolome, I. Sosnowska, and R. Przenios, Phys. Rev. B **55**, 1143 (1997).
[42] F. Wooten, Optical properties of solids (New York, Academic Press, 1972).
[43] A. Kumar, R. C. Rai, N. J. Podraza, S. Denev, M. Ramirez, Y. H. Chu, L. W. Martin, J. Ihlefeld, T. Heeg, J. Schubert, D. G. Schlom, J. Orenstein, R. Ramesh, R. W. Collins, J. L. Musfeldt and V. Gopalan, Appl. Phys. Lett. 92, 121915 (2008)
[44] Yu. F. Popov, A. K. Zvezdin, G. P. Vorob'ev, A. M. Kadomtseva, V. A. Murashev, and D. N. Rakov, JETP Lett. **57**, 69 (1993).
[45] Magnetic anisotropy is responsible for easy and hard magnetization axes in $BiFeO_3$, and as a result, the transition field is different when magnetic field is applied in different orientation[22,44].
[46] M. K. Singh, R. S. Katiyar, and J. F. Scott, J. Phys. Condens. Matter **20**, 4 (2008).
[47] J. F. Scott, M. K. Singh, and R. S. Katiyar, J. Phys. Condens. Matter **20**, 322203 (2008).
[48] I. Dzyaloshinsky, J. Phys. Chem. Solids **4**, 241 (1958).
[49] T. Moriya, Phys. Rev. **120**, 91 (1960).
[50] B. Ruette, S. Zvyagin, A. P. Pyatakov, A. Bush, J. F. Li, V. I. Belotelov, A. K. Zvezdin, and D. Viehland, Phys.

Rev. B **69**, 064114 (2004).
[51] $B_{C,ave}$ curve can be fitted with exponential decay function as: $21.2e^{-17.3x}$, indicating the critical field vanishes rapidly with chemical substitution.
[52] J. Lu, A. Günther, F. Schrettle, F. Mayr, S. Krohns, P. Lunkenheimer, A. Pimenov, V. D. Travkin, A. A. Mukhin, A. Loidl, Eur. Phys. J. B **75**, 451 (2010).
[53] N. W. Ashcroft, and N. D. Mermin, Solid state physics (Brooks Cole, 1976).